MODELLING LAMINAR TRANSPORT PHENOMENA IN A CASSON RHEOLOGICAL FLUID FROM AN ISOTHERMAL SPHERE WITH PARTIAL SLIP

by

Annasagaram SUBBARAO [a], ***Vallampati R. PRASAD*** [b*], ***Nandanoor BHASKAR REDDY*** [a], ***and Osman ANWER BEG*** [c]

[a] Department of Mathematics, Sri Venkateswara University, Tirupathi, India
[b] Department of Mathematics, Madanapalle Institute of Technology and Science, Madanapalle, India
[c] Aerospace Engineering, Sheffield Hallam University, Sheffield, UK

Original scientific paper
DOI:10.2298/TSCI120828098S

The laminar boundary layer flow and heat transfer of Casson non-Newtonian fluid from a permeable isothermal sphere in the presence of thermal and hydrodynamic slip conditions is analysed. The surface of the sphere is maintained at a constant temperature. The boundary layer conservation equations, which are parabolic in nature, are normalized into non-similar form and then solved numerically with the well-tested, efficient, implicit, stable Keller-box finite-difference scheme. Increasing velocity slip induces acceleration in the flow near the surface of the sphere and the reverse effect further from the surface. Increasing velocity slip consistently enhances temperatures throughout the boundary layer regime. An increase in thermal slip parameter strongly decelerates the flow and also reduces temperatures in the boundary layer regime. An increase in Casson rheological parameter acts to elevate considerably the skin friction (non-dimensional wall shear stress) and this effect is pronounced at higher values of tangential co-ordinate. Temperatures are however very slightly decreased with increasing values of Casson rheological parameter. Increasing mass flow injection (blowing) at the sphere surface causes a strong acceleration, whereas increasing suction is found to induce the opposite effect. The study finds applications in rheological chocolate food processing.

Key words: *non-Newtonian fluid mechanics, Casson model, yield stress, slip condition, Keller-box numerical method, heat transfer, skin friction, Nusselt number, boundary layers, chocolate food processing*

Introduction

Non-Newtonian transport phenomena arise in many branches of process mechanical, chemical, and materials engineering. Such fluids exhibit shear-stress-strain relationships which diverge significantly from the classical Newtonian (Navier-Stokes) model. Most non--Newtonian models involve some form of modification to the momentum conservation equations. These include power-law fluids [1], viscoelastic fluids including Maxwell upper-convected models [2], Walters-B short memory models [3, 4], Oldroyd-B models [5], differen-

* Corresponding author; e-mail: rcpmaths@gmail.com

tial Reiner-Rivlin models [6, 7], and Bingham plastics [8]. The flow of non-Newtonian fluids in the presence of heat transfer is an important research area due to its relevance to the optimized processing of chocolate [9], toffee, and other foodstuffs [10]. The Casson model has proved more successful in comparison with the various rheological models developed in biotechnology and food engineering. This simple, yet elegant rheological model was introduced originally [11] to simulate industrial inks. This model [12] constitutes a plastic fluid model which exhibits shear thinning characteristics, yield stress and high shear viscosity. The Casson fluid model is reduced to a Newtonian fluid at a very high wall shear stress *i. e.* when the wall stress is much greater than yield stress. This fluid model also approximates reasonably well the rheological behaviour of other liquids including physiological suspensions, foams, cosmetics, syrups, *etc*.

A number of theoretical, numerical and experimental studies of transport phenomena in Casson fluids have been presented in a variety of areas including biomedical engineering [13-15] and manufacturing technology [16]. Neofytou [17] studied computationally the flow characteristics of both power-law and Casson fluids in symmetric sudden expansions, showing that the critical generalised Reynolds number of transition from symmetry to asymmetry and subsequently the inverse dimensionless wall shear stress are linearly related to the dimensionless wall shear rate. Kandasamy *et al.* [18] studied numerically the thermal convection in concentric annuli using a Casson model. Mass transfer in a Casson flowing through an annular geometry was examined by Nagarani *et al.* [19] who derived analytical solutions and also considered boundary absorption effects. Hemodynamic simulations of Casson blood flow in complex arterial geometries were studied by Shaw *et al.* [20]. Attia and Sayed-Ahmed [21] studied the unsteady hydromagnetic Couette flow and heat transfer in a Casson fluid using the Crank-Nicolson implicit method, showing that Casson number (dimensionless yield stress parameter) controls strongly the velocity overshoot and has a significant effect on the time at which the overshoot arises. Hayat *et al.* [22] obtained homotopic solutions for stagnation-point flow and heat transfer of a Casson fluid along a stretching surface, also considering viscous heating effects. Mustafa *et al.* [23] very recently investigated also with a homotopy method, the transient dissipative flow and heat transfer of a Casson fluid over a moving flat plate with a parallel free stream, showing that surface shear stress and surface heat transfer are increased with the Casson fluid parameter and also Eckert number (viscous heating parameter).

The studies invariably assumed the "no-slip" condition at the boundary. Slip effects have however shown to be significant in certain industrial thermal problems and manufacturing fluid dynamics systems. Sparrow and Lin [24] presented the first significant investigation of laminar slip-flow heat transfer for tubes with uniform heat flux. These studies generally indicated that velocity slip acts to enhance heat transfer whereas thermal slip (or "temperature jump") depresses heat transfer. Many studies have appeared in recent years considering both hydrodynamic and thermal slip effects. Interesting articles of relevance to process mechanical engineering include Larrode *et al.* [25] who studied thermal/velocity slip effects in conduit thermal convection, Spillane [26] who examined sheet processing boundary layer flows with slip boundary conditions and Crane and McVeigh [27] which studied slip hydrodynamics on a micro-scale cylindrical body. Further studies in the context of materials processing include Crane and McVeigh [28]. Studies of slip flows from curved bodies include Wang and Ng [29] which studied using asymptotic analysis the slip hydrodynamics from a stretching cylinder. Wang [30] has also examined stagnation slip flow and heat transfer from an axially moving cylinder showing that heat transfer increases with slip, Prandtl number and Reynolds number, and that in the case of large slip, the flow field decays exponentially into potential flow.

The objective of the present paper is to investigate the laminar boundary layer flow and heat transfer of a Casson rheological fluid past an isothermal sphere. Mathematical modelling through equations of continuity and motion leads to dimensionless non-linear coupled differential boundary layer equations. The velocity and thermal slip conditions along with conservation law of mass, momentum and energy completes the problems formulation for velocity components and temperature. The considered slip conditions are important in non--Newtonian foodstuff transport processes [10, 12] which often exhibit wall slip. It has been experimentally verified that fluid possesses non-continuum features such as slip flow when the molecular mean free path length of fluid is comparable to a representative geometrical length of the system being studied *e. g.* diameter of a cylindrical body. A finite difference numerical solution is presented for the transformed boundary layer equations and a parametric study is conducted the Prandtl number, Casson rheological parameter, wall suction/injection, and velocity/thermal slip effects on the momentum and heat transfer characteristics conducted. The present problem has to the authors' knowledge not appeared thus far in the scientific literature.

Mathematical model

Consider the steady, laminar, 2-D, viscous, incompressible, buoyancy-driven convection heat transfer flow from an isothermal sphere embedded in a Casson non-Newtonian fluid. Figure 1 shows the flow model and physical co-ordinate system. Here x is measured along the surface of the sphere and y is measured normal to the surface, respectively, and r is the radial distance from symmetric axes to the surface. $r = a \sin(x/a)$, where a is the radius of the sphere. The gravitational acceleration, g acts downwards.

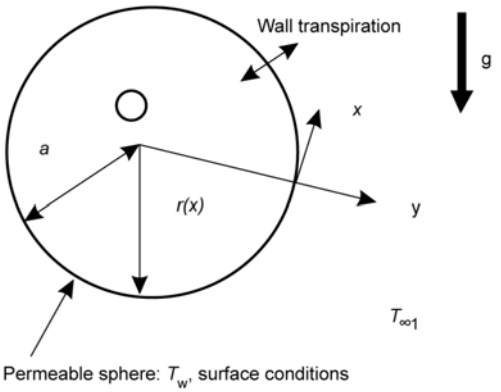

Figure 1. Physical model and co-ordinate system

Both the sphere and the fluid are maintained initially at the same temperature. Instantaneously they are raised to a temperature $T_w > T_\infty$, the ambient temperature of the fluid which remains unchanged. The rheological equation of state for an isotropic flow of Casson fluid, following Steffe [10] in tensorial notation may be stated:

$$\tau_{ij} = \begin{cases} 2\left(\mu_B + \dfrac{p_y}{\sqrt{2\pi}}\right) e_{ij}, & \pi \geq \pi_c \\ 2\left(\mu_B + \dfrac{p_y}{\sqrt{2\pi_c}}\right) e_{ij}, & \pi < \pi_c \end{cases} \tag{1}$$

where $\pi = e_{ij}e_{ij}$ and e_{ij} is the $(i, j)^{th}$ component of deformation rate, π – the product of the component of deformation rate with itself, π_c – a critical value of this product based on the non--Newtonian model, μ_B – the plastic dynamic viscosity of non-Newtonian fluid, and p_y – the yield stress of fluid. In line with the approach of Yih [31] and introducing the boundary layer approximations, the equations for mass continuity, momentum and energy, can be written:

$$\frac{\partial(ru)}{\partial x}+\frac{\partial(rv)}{\partial y}=0 \tag{2}$$

$$u\,\frac{\partial u}{\partial x}+v\,\frac{\partial u}{\partial y}=\nu\left(1+\frac{1}{\beta}\right)\frac{\partial^2 u}{\partial y^2}+g\Omega(T-T_\infty)\sin\left(\frac{x}{a}\right) \tag{3}$$

$$u\,\frac{\partial T}{\partial x}+v\,\frac{\partial T}{\partial y}=\alpha\,\frac{\partial^2 T}{\partial y^2} \tag{4}$$

where u and v are the velocity components in the x- and y-directions, respectively, ν – the kinematic viscosity of the conducting fluid, β – the non-Newtonian Casson parameter, α – the thermal diffusivity, and T – the temperature.

The boundary conditions are prescribed at the sphere surface and the edge of the boundary layer regime, respectively:

$$\begin{aligned}&\text{at } y=0, \qquad u=N_0\left(1+\frac{1}{\beta}\right)\frac{\partial u}{\partial y}, \qquad v=-\vec{V}_w, \qquad T=T_w+K_0\,\frac{\partial T}{\partial y}\\ &\text{as } y\to\infty, \qquad u\to 0, \qquad T\to T_\infty\end{aligned} \tag{5}$$

where N_0 is the velocity slip factor and K_0 – the thermal slip factor. For $N_0 = 0 = K_0$, one can recover the no-slip case.

The stream function ψ is defined by $ru=\partial(r\psi)/\partial y$ and $rv=-\partial(r\psi)/\partial x$, and therefore, the continuity equation is automatically satisfied. In order to write the governing equations and the boundary conditions in dimensionless form, the following non-dimensional quantities are introduced:

$$\begin{aligned}&\xi=\frac{x}{a}, \qquad \eta=\frac{y}{a}\sqrt[4]{\mathrm{Gr}}, \qquad f(\xi,\eta)=\frac{\psi}{\nu\xi\sqrt[4]{\mathrm{Gr}}}, \qquad \mathrm{Pr}=\frac{\nu}{\alpha},\\ &\theta(\xi,\eta)=\frac{T-T_\infty}{T_w-T_\infty}, \qquad \mathrm{Gr}=\frac{g\Omega(T_w-T_\infty)a^3}{\nu^2}, \qquad \beta=\mu_B\,\frac{\sqrt{2\pi_c}}{\rho_y}\end{aligned} \tag{6}$$

where ρ is the mass density, T_∞ – the free stream temperature, and $\vec{V}_w$ – the uniform blowing/suction velocity.

In view of eq. (6), eqs. (2)-(4) reduce to the following coupled, non-linear, dimensionless partial differential equations for momentum and energy for the regime:

$$\left(1+\frac{1}{\beta}\right)f'''+\left(1+\xi\cot\xi\right)ff''-f'^2+\frac{\sin\xi}{\xi}\,\theta=\xi\left(f'\,\frac{\partial f'}{\partial\xi}-f''\,\frac{\partial f}{\partial\xi}\right) \tag{7}$$

$$\frac{\theta''}{\mathrm{Pr}}+\left(1+\xi\cot\xi\right)f\theta'=\xi\left(f'\,\frac{\partial f'}{\partial\xi}-f''\,\frac{\partial f}{\partial\xi}\right) \tag{8}$$

The transformed dimensionless boundary conditions are:

$$\begin{aligned}&\text{at } \eta=0, \qquad f_w=S, \qquad f'=\left(1+\frac{1}{\beta}\right)S_f f''(0), \qquad \theta=1+S_T\theta'(0)\\ &\text{as } \eta\to\infty, \qquad f'\to 0, \qquad \theta\to 0\end{aligned} \tag{9}$$

In these equations, the primes denote the differentiation with respect to η, the dimensionless radial co-ordinate, and ξ is the dimensionless tangential co-ordinate, Pr = ν/α the Prandtl number, $S_f = (N_0 \mathrm{Gr}^{1/4})/a$, and $S_T = (K_0 \mathrm{Gr}^{1/4})/a$ are the non-dimensional velocity and thermal slip parameters respectively and $f_w = S = (-\vec{V}_w a)/(\nu \mathrm{Gr}^{1/4})$ is the blowing/suction parameter $f_w < 0$ for $\vec{V}_w > 0$ (the case of blowing), and $f_w > 0$ for $\vec{V}_w < 0$ (the case of suction). Of course the special case of a solid sphere surface corresponds to $f_w = 0$. Here we assumed the typical values $K_0 = 0.5$, $N_0 = 0.25$, Gr =16, and $a = 1.0$ for finding the non-dimensional velocity and thermal slip parameters.

The engineering design quantities of physical interest include the skin-friction coefficient and Nusselt number, which are given by:

$$\frac{1}{2} C_f \sqrt[4]{\frac{1}{\mathrm{Gr}^3}} = \left(1 + \frac{1}{\beta}\right) \xi f''(0) \tag{10}$$

$$\frac{\mathrm{Nu}}{\sqrt[4]{\mathrm{Gr}}} = -\theta'(0) \tag{11}$$

Numerical solution

The present analysis integrates the system of eqs. (7) and (8) with the boundary conditions eq. (9) by the implicit finite difference approximation together with the modified Keller box method of Cebeci and Bradshaw [32]. For the sake of brevity, the numerical method is not described. Computations were carried out with $\Delta\xi = 0.1$; the first step size $\Delta\eta = 0.02$. The requirement that the variation of the velocity and temperature distribution is less than 10^{-5} between any two successive iterations is employed as the criterion convergence. In most laminar boundary layer flows, a step size of $\Delta\eta = 0.02$ to 0.04 is sufficient to provide accurate and comparable results. In fact in the present problem, we can even go up to $\Delta\eta = 0.1$ and still get accurate and comparable results. This particular value of $\Delta\eta = 0.1$ has also been used successfully by Merkin [33]. A uniform grid across the boundary is quite satisfactory for most laminar flow calculations, especially in laminar boundary layer. However, the Keller-box method is unique in which various spacing in both η and ξ directions can be used, Aldoss *et al.* [34].

Results and discussion

Comprehensive solutions have been obtained and are presented in figs. 2-19. The numerical problem comprises two independent variables (ξ, η), two dependent fluid dynamic variables (f, θ), and six thermo-physical and body force control parameters, namely Pr, S_f, S_T, β, f_w, and ξ. In the present computations, the following default parameters are prescribed (unless otherwise stated): Pr = 10.0, S_f= 0.5, S_T= 1.0, β = 1.0, f_w = 0.5, and ξ = 1.0.

In figs. 2 and 3, the influence of velocity slip parameter on velocity and temperature distributions is illustrated. Dimensionless velocity component (fig. 2) at the wall is strongly reduced with an increase in slip parameter, S_f. There will be a corresponding decrease in the momentum (velocity) boundary layer thickness.

The influence of S_f is evidently more pronounced closer to the sphere surface ($\eta = 0$). Further from the surface, there is a transition in velocity slip effect, and the flow is found to be accelerated markedly. Smooth decays of the velocity profiles are observed into the free stream demonstrating excellent convergence of the numerical solution. These trends in the response of velocity field in external thermal convection from a cylinder were also observed by Wang and Ng [29], and Wang [30]. Furthermore the acceleration near the wall with

increasing velocity slip effect has been computed by Crane and McVeigh [28] using asymptotic methods, as has the retardation in flow further from the wall. The switch in velocity slip effect on velocity evolution has also been observed for the case of a power-law rheological fluid by Ajadi *et al.* [35]. Figure 3 indicates that an increase in velocity slip parameter significantly enhances temperature in the flow field and thereby increases thermal boundary layer thickness enhances. This will result therefore in the transport of more thermal energy from the sphere surface to the Casson fluid and will therefore accentuate heat transfer to the fluid, as noted also by Wang [30]. Temperature profiles consistently decay monotonically from a maximum at the sphere surface to the free stream. All profiles converge at large value of radial co-ordinate, again showing that convergence has been achieved in the numerical computations. A similar pattern of thermal response to that computed in fig 3. for a wide range of velocity slip parameters has been noted by Aziz [36] who has indicated also that temperature is enhanced since increasing velocity slip parameter decreases shear stresses and this permits a more effective transfer of heat from the wall to the fluid regime.

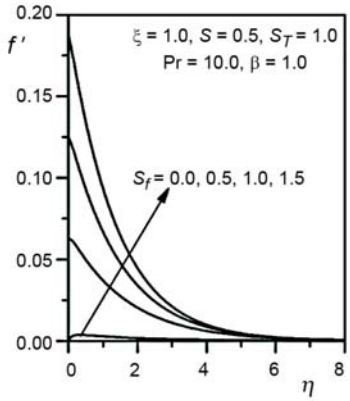

Figure 2. Influence of S_f on velocity profiles

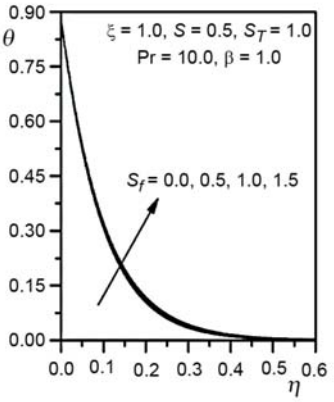

Figure 3. Influence of S_f on temperature profiles

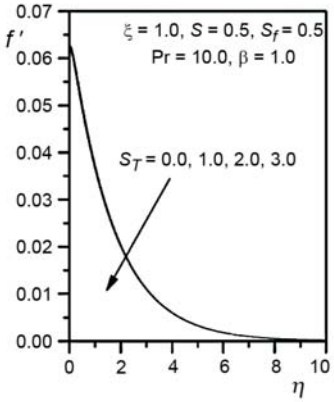

Figure 4. Influence of S_T on velocity profiles

In figs. 4 and 5, the variation of velocity and temperature with the transverse co-ordinate (η), with increasing thermal slip parameter S_T is depicted. The response of velocity is much more consistent than for the case of changing velocity slip parameter (fig. 2) – it is strongly decreased for all locations in the radial direction. The peak velocity accompanies the case of no thermal slip ($S_T = 0$). The maximum deceleration corresponds to the case of strongest thermal slip ($S_T = 3$). Temperatures (fig. 5) are also strongly depressed with increasing thermal slip. The maximum effect is observed at the wall. Further into the free stream, all temperature profiles converge smoothly to the vanishing value. The numerical computations correlate well with the results of Larrode *et al.* [25] who also found that temperature is strongly lowered with increasing thermal slip and that this is attributable to the decrease in heat transfer from the wall to the fluid regime, although they considered only a Newtonian fluid.

Figures 6 and 7 depict the influence Casson fluid parameter, β on velocity and temperature profiles. This parameter features in the shear term in the momentum boundary layer eq. (7), and also in the velocity boundary condition eq. (9). For Newtonian flow, yield stress p_y is zero, and $\beta = \mu_B \sqrt{\pi_c}/p_y \to \infty$ *i. e.* the appropriate term in eq. (7) reduces from $(1 + 1/\beta) f''' \to 1$. Similarly the velocity boundary condition in eq. (9) reduces from $(1 + 1/\beta)\, S_f f''(0) \to S_f f''(0)$. An increase in β implies a decrease therefore in yield stress of the Casson fluid. This effectively facilitates flow of the fluid *i. e*. accelerates the boundary layer flow close to

the sphere surface, as demonstrated by fig. 6. Since the Casson parameter is also present in the wall boundary condition, the acceleration effect is only confined to the region close to the sphere surface. Further from this zone, the velocity slip factor, S_f will exert a progressively reduced effect and an increase in Casson parameter, β will manifest with a deceleration in the flow. However, the dominant influence of β, is near the wall and is found to be assistive to momentum development (with larger β values the fluid is closer in behaviour to a Newtonian fluid and further departs from plastic flow). Only a very small decrease in temperature is observed with a large enhancement in Casson fluid parameter, as shown in fig. 7. The Casson parameter does not arise in the thermal boundary layer eq. (8), nor does it feature in the thermal boundary conditions. The influence on temperature field is therefore experienced indirectly via coupling of the thermal eq. (8) with the momentum eq. (7). Similar behaviour to the computations shown in figs. 6 and 7, has been observed by Attia and Sayed-Ahmed [21] who also observed acceleration in Casson fluid flow near a curved surface, and additionally by Mustafa *et al.* [23] who also observed an elevation in velocities near the wall and a slight reduction in temperatures throughout the boundary layer regime.

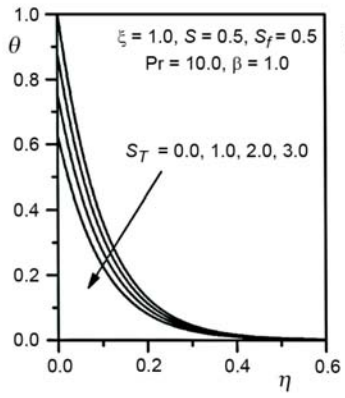

Figure 5. Influence of S_T on temperature profiles

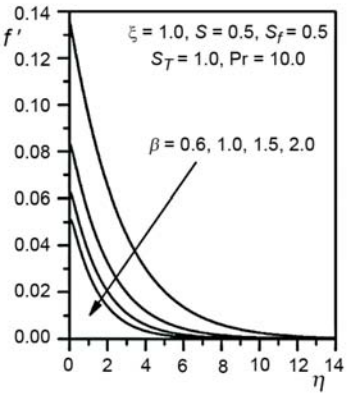

Figure 6. Influence of β on velocity profiles

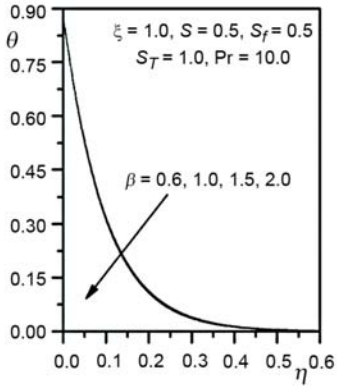

Figure 7. Influence of β on temperature profiles

Figures 8 and 9, present the effect of Prandtl number on the velocity and temperature profiles along the radial direction, normal to the sphere surface. Prandtl number embodies the ratio of viscous diffusion to thermal diffusion in the boundary layer regime.

The mentioned figures also express the ratio of the product of specific heat capacity and dynamic viscosity, to the fluid thermal conductivity. When the Prandtl number is high, viscous diffusion rate exceeds thermal diffusion rate. An increase in the Prandtl number from 0.01 through 0.1, 0.3, 0.5, 0.7 to 1.0, is found to significantly depress velocities (fig. 8) and this trend is sustained throughout the regime *i. e.* for all values of the radial co-ordinate, η. For Pr < 1, thermal diffusivity exceeds momentum diffusivity *i. e.* heat will diffuse faster than momentum. Therefore for lower Pr fluids (*e. g.* Pr = 0.01 which physically correspond to liquid metals), the flow will be accelerates whereas for greater Pr fluids (*e. g.* Pr = 1) it will be strongly decelerated, as observed in fig. 8. For Pr = 1.0, both the viscous and energy diffusion rates will be the same as will the thermal and velocity boundary layer thicknesses. This case can be representative of food stuffs *e. g.* low-density polymorphic forms of chocolate suspensions, as noted by Steffe [10]. Temperature is found to be strongly reduced with increasing Prandtl number. For the case of Pr = 0.01, the decay is almost exactly linear. For larger Pr

values, the decay is found to be increasingly monotonic. Therefore for lower thermal conductivity fluids (as typified by liquid chocolate and other foodstuffs), lower temperatures are observed throughout the boundary layer regime.

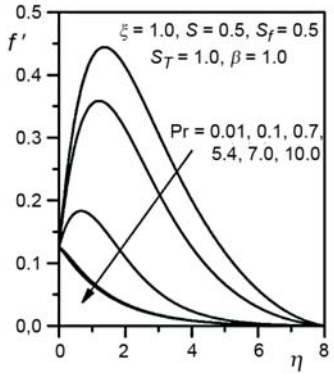

Figure 8. Influence of Pr on velocity profiles

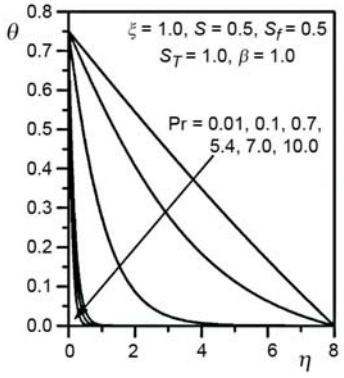

Figure 9. Influence of Pr on temperature profiles

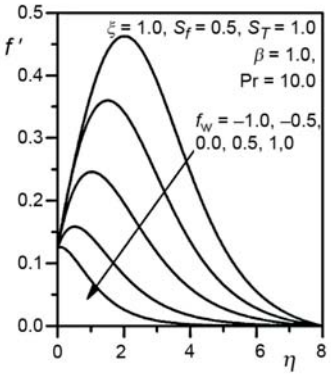

Figure 10. Influence of f_w on velocity profiles

Figures 10 and 11, illustrate the influence of wall transpiration on the velocity and temperature functions with radial distance, η. With an increase in suction ($f_w > 0$) the velocity is clearly decreased *i. e.* the flow is decelerated. Increasing suction causes the boundary layer to adhere closer to the flow and destroys momentum transfer; it is therefore an excellent control mechanism for stabilizing the external boundary layer flow on the circular sphere. Conversely with increased blowing *i. e.* injection of fluid via the sphere surface in to the porous medium regime, ($f_w < 0$), the flow is strongly accelerated *i. e.* velocities are increased. As anticipated the case of a solid sphere ($f_w = 0$) falls between the weak suction and weak blowing cases. Peak velocity is located, as in the figures described earlier, at close proximity to sphere surface.

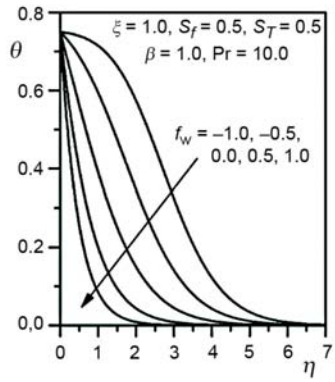

Figure 11. Influence of f_w on temperature profiles

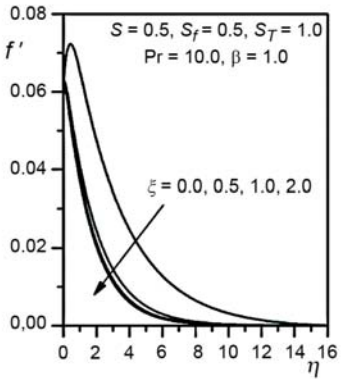

Figure 12. Influence of ξ on velocity profiles

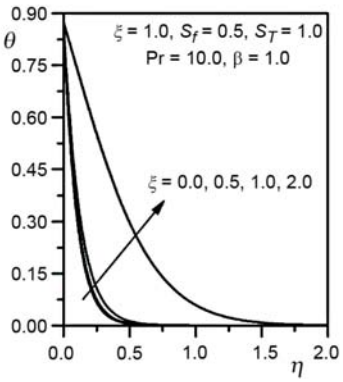

Figure 13. Influence of ξ on temperature profiles

With a decrease in blowing and an increase in suction the peaks progressively displace closer to the sphere surface, a distinct effect described in detail in several studies of non-Newtonian boundary layers [1, 3, 7, 22, 23]. Temperature, θ, is also elevated considerably with increased blowing at the sphere surface and depressed with increased suction. The tem-

perature profiles, once again assume a continuous decay from the sphere surface to the free stream, whereas the velocity field initially ascends, peaks and then decays in to the free stream. The strong influence of wall transpiration (*i. e.* suction or injection) on boundary layer variables is clearly highlighted. Such a mechanism is greatly beneficial in achieving flow control and regulation of heat and mass transfer characteristics in food processing from a cylindrical geometry.

Figures 12 and 13, the variation of velocity and temperature fields with different transverse co-ordinate, ξ, is shown. In the vicinity of the sphere surface, velocity (f') is found to be maximized closer to the lower stagnation point and minimized with progressive distance away from it, *i. e.* the flow is decelerated with increasing ξ. However further from the wall, this trend is reversed and a slight acceleration in the flow is generated with greater distance from the lower stagnation point *i. e.* velocity values are higher for greater values of ξ, as we approach the upper stagnation point temperature, θ is found to noticeably decrease through the boundary layer with increasing ξ values. Evidently the fluid regime is cooled most efficiently at the lower stagnation point and heated more effectively as we progress around the sphere periphery upwards towards the upper stagnation point. These patterns computed for temperature and velocity evolution around the sphere surface are corroborated with many other studies including work on non-Newtonian Casson fluid convection by Kandasamy *et al.* [18] and studies of Newtonian convection from a cylinder by Wang [30], and Prasad *et al.* [37].

Figsures 14 and 15 show the effect of velocity slip parameter S_f on sphere surface shear stress (f'') and local Nusselt number ($-\theta'$) variation. In consistency with the earlier graphs described for velocity evolution, with an increase in S_f, wall shear stress is consistently reduced *i. e.* the flow is decelerated along the sphere surface. Again this trend has been observed by Wang and Ng [29], and Wang [30] using asymptotic methods. There is also a progressive migration in the peak shear stress locations further from the lower stagnation point, as wall slip parameter is increased. The impact of wall slip is therefore significant on the boundary layer characteristics of Casson flow from a cylinder. With an increasing S_f, the local Nusselt number is also considerably decreased and profiles are generally monotonic decays. Maximum local Nusselt number always arises at the sphere surface and is minimized with proximity to the lower stagnation point *i. e.* greater distance from the upper stagnation point. This pattern of behaviour has also been observed and emphasized by Yih [31] for Newtonian flow. In both figures 14 and 15, skin friction coefficient and local Nusselt number are maxim-

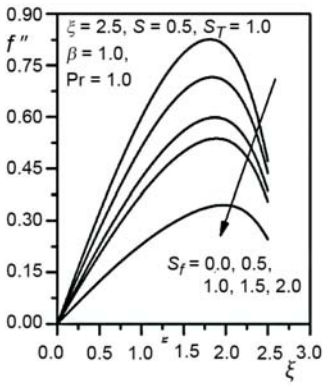

Figure 14. Effect of S_f on the skinfriction coefficient results

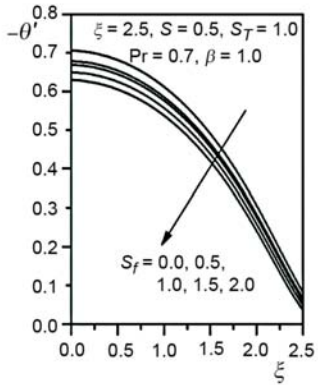

Figure 15. Effect of S_f on the local Nusselt number results

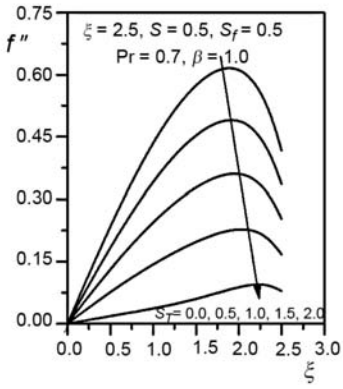

Figure 16. Effect of S_T on the skinfriction coefficients results

ized for the case of no-slip *i. e.* $S_f = 0$, this result concurring with the analyses of Wang [30] and also Hayat *et al.* [22].

Figures 16 and 17 show the effect of thermal slip parameter S_T on dimensionless wall shear stress function *i. e.* skin friction coefficient and local Nusselt number, respectively. Increasing S_T is found to decrease both skin friction coefficient and local Nusselt number. A similar set of profiles is computed as in fig. 14 for velocity distributions, and we observe that with increasing thermal slip, peak velocities are displaced closer to the lower stagnation point. For lower values of thermal slip, the plots are also similar to those in fig. 15, and have a parabolic nature; however with S_T values > 1, the profiles lose their curvature and become increasingly linear in nature. This trend is maximized for the highest value of S_T (= 3.0) for which local Nusselt number is found to be almost invariant with transverse co-ordinate, ξ.

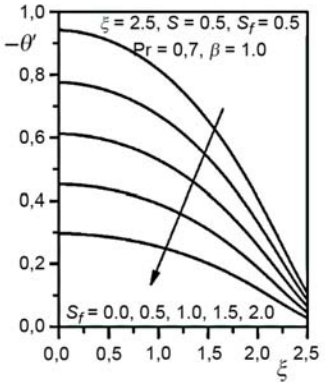

Figure 17. Effect of S_T on the local Nusselt number results

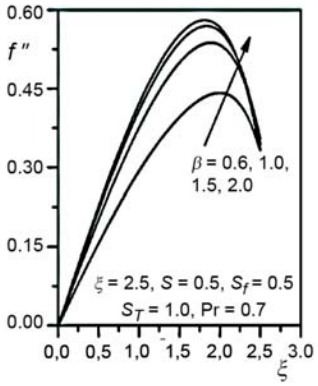

Figure 18. Effect of β on the skinfriction coefficient results

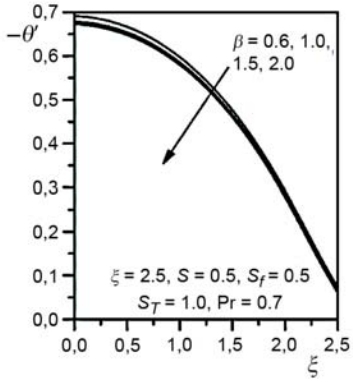

Figure 19. Effect of β on the local Nusselt number results

Figures 18 and 19 illustrate the effect of Casson fluid parameter, β, on skin friction coefficient and local Nusselt number, respectively. With an increase in β the skin friction coefficient increases, since as computed earlier, the flow velocity is enhanced with higher values of β. Larger β values correspond to a progressive decrease in yield stress of the Casson fluid *i. e.* a reduction in rheological characteristics. With higher β the flow approaches closer to Newtonian behaviour and the fluid is able to shear faster along the sphere surface. Local Nusselt number is conversely found to decrease slightly as Casson fluid parameter is increased. This concurs with the earlier computation (fig. 7) on temperature distribution. With increasing β values, less heat is transferred from the sphere surface to the fluid regime, resulting in lower temperatures in the regime external to the sphere and lower local Nusselt numbers, as observed in fig. 19.

Conclusions

Numerical solutions have been presented for the transport phenomena *i. e.* combined heat and flow of Casson rheological fluid external to an isothermal sphere, with suction/injection effects and velocity/thermal slip. The model has been developed to simulate foodstuff transport processes in industrial manufacturing operations. A robust, extensively-validated, implicit finite difference numerical scheme has been implemented to solve the transformed, dimensionless velocity and thermal boundary layer equations, subject to physically realistic boundary conditions. The computations have shown that:

- Increasing the velocity slip parameter, S_f, reduces the velocity near the sphere surface and also skin friction coefficient and also increases temperature and decreases local Nusselt number.
- Increasing the thermal slip parameter, S_T, decreases velocity and skin friction coefficient and also reduces temperature for all values of radial co-ordinate *i. e.* throughout the boundary layer regime, and furthermore decreases local Nusselt number.
- Increasing the Casson fluid parameter, β, increases the velocity near the sphere surface but decreases velocity further from the sphere, and also fractionally lowers the temperature throughout the boundary layer regime.
- Increasing the Casson fluid parameter, β, strongly increases the wall shear stress (skin friction coefficient) and slightly decreases the local Nusselt number, with the latter more significantly affected at large distances from the lower stagnation point *i. e.* higher values of transverse co-ordinate.
- Increasing suction at the sphere surface ($f_w > 0$) decelerates the flow whereas increasing injection ($f_w < 0$, *i. e.* blowing) induces a strong acceleration.
- Increasing suction at the sphere surface ($f_w > 0$) reduces temperature whereas increasing injection ($f_w < 0$ *i. e.* blowing) induces the opposite response and elevates temperature.
- Increasing transverse co-ordinate, ξ, depresses velocity near the sphere surface but enhances velocity further from the sphere, whereas it continuously decreases temperature throughout the boundary layer.

The current study has been confined to steady-state flow *i. e.* ignored transient effects [4] and also neglected thermal radiation heat transfer effects [37]. These aspects are also of relevance to rheological food processing simulations and will be considered in future investigations.

Acknowledgments

The authors are grateful to both reviewers for their constructive comments which have helped to improve the present article.

Nomenclature

a – radius of the sphere
C_f – skin friction coefficient
f – non-dimensional steam function
Gr – Grashof number
g – acceleration due to gravity
K_0 – thermal slip factor
N_0 – velocity slip factor
Nu – local Nusselt number
Pr – Prandtl number
$r(x)$ – radial distance from symmetrical axis to surface of the sphere
S_f – non-dimensional velocity slip parameter
S_T – non-dimensional thermal slip parameter
T – temperature
u, v – non-dimensional velocity components along the x- and y-directions, respectively
$\vec{V}$ – the linear (translational) fluid velocity vector
x – stream wise co-ordinate
y – transverse co-ordinate

Greek symbols

α – thermal diffusivity
β – the non-Newtonian Casson Parameter
η – the dimensionless radial co-ordinate
θ – non-dimensional temperature
μ – dynamic viscosity
ν – kinematic viscosity
ξ – the dimensionless tangential co-ordinate
ρ – mass density
ψ – dimensionless stream function
Ω – the coefficient of thermal expansion
Λ – the local inertial drag coefficient (Forchheimer parameter)

Subscripts

w – conditions on the wall
∞ – free stream conditions

References

[1] Anwar Beg., O., *et al.*, Modelling of Ostwald-deWaele Non-Newtonian Flow over a Rotating Disk in a Non-Darcian Porous Medium, *International Journal Applied Mathematics and Mechanics, 8* (2012), 13, pp. 46-67
[2] Anwar Beg., O., Makinde, O. D., Viscoelastic Flow and Species Transfer in a Darcian High-Permeability Channel, *Journal of Petroleum Science and Engineering, 76* (2011), 3-4, pp. 93-99
[3] Gouse Mohiddin, S., *et al.*, Numerical Study of Unsteady Free Convective Heat and Mass Transfer in a Walters-B Viscoelastic Flow along a Vertical Cone, *International Journal of Applied Mathematics and Mechanics, 6* (2010), 15, pp. 88-114
[4] Prasad, V. R., *et al*., Unsteady Free Convection Heat and Mass Transfer in a Walters-B Viscoelastic Flow past a Semi-Infinite Vertical Plate: a Numerical Study, *Thermal Science, 15* (2011), Suppl. 2, pp. S291-S305
[5] Tripathi, D., *et al*., Homotopy Semi-Numerical Simulation of Peristaltic Flow of Generalised Oldroyd-B Fluids with Slip Effects, *Computer Methods in Biomechanics Biomedical Engineering, 17* (2014), 4, pp. 433-442
[6] Anwar Beg, O. A., *et al*., Numerical Study of Heat Transfer of a Third Grade Viscoelastic Fluid in Non-Darcian Porous Media with Thermophysical Effects, *Physica Scripta, 77* (2008), 6, pp. 1-11
[7] Rashidi, M. M., *et al.*, A Study of Non-Newtonian Flow and Heat Transfer over a Non-Isothermal Wedge Using the Homotopy Analysis Method, *Chemical Engineering Communications, 199* (2012), 2, pp. 231-256
[8] Huilgol, R. R., You, Z., Application of the Augmented Lagrangian Method to Steady Pipe Flows of Bingham, Casson and Herschel-Bulkley Fluids, *Journal of Non-Newtonian Fluid Mechanics, 128* (2005), 2-3, pp. 126-143
[9] Wilson, L. L., *et al*., Yield Stresses in Molten Chocolates, *Journal of Texture Studies, 24* (1993), 3, pp. 269-286
[10] Steffe. J. F., *Rheological methods in Food Process Engineering*, 2nd ed., Freeman Press, East Lansing, Mich., USA, 2001
[11] Casson. N., *A Flow Equation for Pigment Oil-Suspensions of the Printing Ink Type*, Rheolgy of Disperse Systems (Ed. C. C. Mill), Pergamon Press, London, 1959, pp. 84
[12] Bird, R. B., *et al.*, The Rheology and Flow of Viscoplastic Materials, *Reviews in Chemical Engineering, 1* (1983), pp. 1-83
[13] Chaturani. P., Ponnalagarsamy, R., Pulsatile Flow of Casson's Fluid through Stenosed Arteries with Applications to Blood Flow, *Biorheology, 23* (1986), 5, pp. 499-511
[14] Das, B., Batra, R. L., Secondary Flow of a Casson Fluid in a Slightly Curved Tube, *International Journal of Non-Linear Mechanics, 28* (1993), 5, pp. 567-580
[15] Dash, R. K., *et al.*, Shear-Augmented Dispersion of a Solute in a Casson Fluid Flowing in a Conduit, *Annals of Biomedical Engineering, 28* (2000), 4, pp. 373-385
[16] Batra, R. L., Das, B., Flow of Casson Fluid between Two Rotating Cylinders, *Fluid Dynamics Research, 9* (1992), 1-3, pp. 133-141
[17] Neofytou. P., Transition to Asymmetry of Generalised Newtonian Fluid Flows through a Symmetric Sudden Expansion, *Journal of Non-Newtonian Fluid Mechanics, 133* (2006), 2-3, pp. 132-140
[18] Kandasamy, A., *et al*., Entrance Region Flow Heat Transfer in Concentric Annuli for a Casson Fluid, International Conference of Thermal Issues in Emerging Technologies, Theory and Application (ThETA), Cairo, Egypt, 2007
[19] Nagarani, P., *et al.*, On the Dispersion of a Solute in a Casson Fluid Flow in an Annulus with Boundary Absorption, American Conference of Applied Mathematics (MATH'08), Harvard University, Harvard, Mass., USA, 2008, pp. 265-273
[20] Shaw, S., *et al.*, Pulsatile Casson Fluid Flow Through a Stenosed Bifurcated Artery, *International Journal of Fluid Mechanics Research, 36* (2009), 1, pp. 43-63
[21] Attia, H., Sayed-Ahmed, M. E., Transient MHD Couette Flow of a Casson Fluid between Parallel Plates with Heat Transfer, *Italian Journal of Pure Applied Mathematics, 27* (2010), pp. 19-38
[22] Hayat, T., *et al.*, Stagnation-Point Flow and Heat Transfer of a Casson Fluid towards a Stretching Sheet, *Zeitschrift für Naturforschung, 67a* (2012), 1-2, pp. 70-76
[23] Mustafa, M., *et al.*, Unsteady Boundary Layer Flow of a Casson Fluid due to an Impulsively Started Moving Flat Plate, *Heat Transfer-Asian Research, 40* (2011), 6, pp. 563-576

[24] Sparrow, E. M., Lin, S. H., Laminar Heat Transfer in Tubes under Slip-Flow Conditions, *ASME Journal of Heat Transfer, 84* (1962), 4, pp. 363-639
[25] Larrode, F. E., *et al.*, Slip-Flow Heat Transfer in Circular Tubes, *International Journal of Heat Mass Transfer, 43* (2000), 15, pp. 2669-2680
[26] Spillane, S., A Study of Boundary Layer Flow with No-Slip and Slip Boundary Conditions, Ph. D. thesis, Dublin Institute of Technology, Dublin, Ireland, 2007
[27] Crane, L. J., McVeigh, A. G., Slip Flow on A Microcylinder, *Z. Angew. Math. Phys., 61* (2010), 3, pp. 579-582
[28] Crane, L. J., McVeigh, A. G., Uniform Slip Flow on a Cylinder, PAMM: *Proceedings of Applied Mathematics and Mechanics, 10* (2010), 1, pp. 477-478
[29] Wang, C. Y., Ng, C.-O., Slip Flow due to a Stretching Cylinder, *International Journal of Non-Linear Mechanics, 46* (2011), 9, pp. 1191-1194
[30] Wang, C. Y., Stagnation Flow on a Cylinder with Partial Slip – an Exact Solution of the Navier-Stokes Equations, *IMA Journal of Applied Mathematics, 72* (2007), 3, pp. 271-277
[31] Yih, K. A., Viscous and Joule Heating Effects on Non-Darcy MHD Natural Convection Flow over a Permeable Sphere in Porous Media with Internal Heat Generation, *International Communications in Heat and mass Transfer, 27* (2000), 4, pp. 591-600
[32] Cebeci, T., Bradshaw, P., *Physical and Computational Aspects of Convective Heat Transfer*, Springer, New York, USA, 1984
[33] Merkin, J. H., Free Convection Boundary Layer on an Isothermal Horizontal Cylinder, *Proceedings,* ASME/AICHE Heat Transfer Conference, St. Louis, Mo., USA, 1976
[34] Aldoss, T. K., *et al*., MHD Mixed Convection from a Horizontal Circular Cylinder, *Numerical Heat Transfer, Part A, 30* (1996), 4, pp. 379-396
[35] Ajadi, S. O., *et al.,* Slip Boundary Layer Flow of Non-Newtonian Fluid over a Flat Plate with Convective Thermal Boundary Condition, *International Journal of Nonlinear Science, 8* (2009), 3, pp. 300-306
[36] Aziz, A., Hydrodynamic and Thermal Slip Flow Boundary Layers over a Flat Plate with Constant Heat Flux Boundary Condition, *Communications in Nonlinear Science and Numerical Simulation, 15* (2010), 3, pp. 573-580
[37] Prasad, V. R., *et al.*, Thermal Radiation Effects on Magnetohydrodynamic Heat and Mass Transfer from a Horizontal Cylinder in a Variable Porosity Regime, *Journal of Porous Media, 15* (2012), 3, pp. 261-281

Paper submitted: August 28, 2012
Paper revised: May 17, 2013
Paper accepted: July 16, 2013